Nanoscale

p-Block Element-doped Silicon Nanowires for Nitrogen Reduction Reaction: A DFT Study

Journal:	*Nanoscale*
Manuscript ID	NR-ART-05-2021-003448.R1
Article Type:	Paper
Date Submitted by the Author:	n/a

Complete List of Authors:	Guo, Zhongyuan; Dongguan University of Technology, School of Chemical Engineering and Energy Technology; Swinburne University of Technology, Department of Chemistry and Biotechnology Jasin Arachchige, Lakshitha; Dongguan University of Technology, School of Chemical Engineering and Energy Technology; Swinburne University of Technology, Department of Chemistry and Biotechnology Qiu, Siyao; Dongguan University of Technology, School of Chemical Engineering and Energy Technology Zhang, Xiao Li; Zhengzhou University, School of Material Science and Engineering Xu, Yongjun; Dongguan University of Technology, School of Chemical Engineering and Energy Technology Langford, Steven; Swinburne University of Technology, Department of Chemistry and Biotechnology Sun, Chenghua; Swinburne University of Technology, Department of Chemistry and Biotechnology

A table of contents entry

B-doping on 1D SiNWs can reduce N_2 into NH_3 with an ultralow overpotential of 0.34 V and suppressed HER performance.

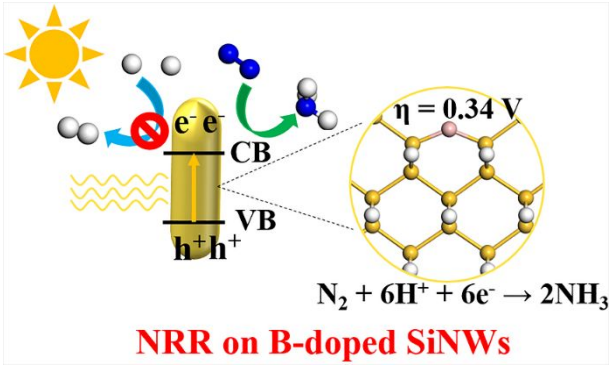

p-Block Element-doped Silicon Nanowires for Nitrogen Reduction Reaction: A DFT Study

Zhongyuan Guo,[a,b] Lakshitha Jasin Arachchige,[a,b] Siyao Qiu,[a,*] Xiaoli Zhang,[c] Yongjun Xu,[a] Steven J. Langford,[b] Chenghua Sun[b,*]

[a] School of Chemical Engineering and Energy Technology, Dongguan University of Technology, Dongguan 523808, China.

[b] Department of Chemistry and Biotechnology, Centre for Translational Atomaterials, Swinburne University of Technology, Hawthorn, Victoria 3122, Australia

[c] School of Material Science and Engineering, Zhengzhou University, Zhengzhou 450001, China.

Keywords: Silicon nanowire; NRR; Electrocatalysis; 1D materials; DFT

[*]***Corresponding author:***

Dr. Siyao Qiu

Address: No. 1 Daxue Rd, Songshan Lake, Dongguan, 523808, China.

Email: qiusy@dgut.edu.cn

Assoc. Prof Chenghua Sun

Address: John St, Hawthorn VIC, 3122, Australia.

Email: chenghuasun@swin.edu.au

Abstract

Photocatalytic nitrogen reduction reaction (NRR) is a promising, green route to chemically reducing N_2 into NH_3 under ambient conditions, correlating to the N_2 fixation process of nitrogenase enzymes. To achieve high-yield NRR with sunlight as the driving force, high-performance photocatalysts are essential. One-dimensional silicon nanowires (1D SiNWs) are a great photoelectric candidate, but inactive for NRR due to its inability to capture N_2. In this study, we proposed SiNWs doped by p-block elements (B, C, P) to tune the affinity to N_2 and demonstrated that two-coordinated boron (B_{2C}) offers an ultra-low overpotential (η) of 0.34 V to catalyze full NRR, which is even much lower than that of flat benchmark Ru(0001) catalysts (η = 0.92 V). Moreover, aspects including suppressed hydrogen evolution reaction (HER), high-spin ground state of the B_{2C} site, and decreased band gap after B-doping ensure the high selectivity and photocatalytic activity. Finally, this work not only shows the potential use of metal-free p-block element-based catalysts, but also would facilitate the development of 1D nanomaterials towards efficient reduction of N_2 into NH_3.

1. Introduction

Ammonia (NH_3) is an extremely important basic industrial chemical used specifically as fertilizer in agricultural production.[1-4] In nature, nitrogenase enzymes in some microorganisms can convert N_2 into NH_3 under ambient conditions.[5-7] Industrially, our society mainly relies on the century-old Haber-Bosch process (HB) as the main artificial nitrogen fixation method, which operates under high energy conditions (300–500℃, 15-25 MPa).[3, 8-10] This traditional method accounts for around 2% of the consumption of the global energy demand, and also emits over 400 million tons of greenhouse gases (CO_2) annually as a result of the consumption of fossil fuels for energy.[10-14] In response to the global challenges of energy crisis and climate change, it is highly urgent that we need to develop a green alternative to HB for sustainable ammonia production. Currently, photocatalytic or electrocatalytic nitrogen reduction methods have been regarded as promising routes. Such methods purport the use of water as a hydrogen provider, and drive N_2 activation and reduction under ambient conditions using renewable energy resources, without significant CO_2 emission.[15-26]

To effectively realize nitrogen fixation, the design of an efficient catalyst is the key challenge. Till now, various metal-based electro(photo)catalysts have been extensively investigated and provided some exciting results.[18, 19, 27-44] However, the Faradic Efficiency (FE) is ultra-low due to the intrinsic interaction between the metals *d* and H-1*s* orbitals besides the high overpotential (η).[45-48] To address this issue, metal-free catalysts have been developed through the engineering of morphology, composition and atomic-scale electronic structures,[48, 49] via heteroatom doping,[50-52] porous structure/network formation,[53-55] transition from bulk materials to low-dimensional materials,[56, 57] and defect introduction.[58, 59] Although both activity and selectivity

have been dramatically improved through previous studies, some of which are even close to metal-based ones, the NRR performance is still far away from pragmatic application.[60]

One-dimensional semiconductor silicon nanowires (1D SiNWs) have received much attention due to attractive properties such as earth abundance, high aspect ratio, tunable physical and electronical properties, chemisorption capacity, facile growth techniques. Importantly, they show utility having been widely used in energy conversion and storage devices.[61-64] Following these successes, SiNWs may be considered as a potential metal-free platform for photocatalytic reactions, albeit the exploration of SiNWs as photocatalysts for NRR has been rarely reported. Such a situation may result from the poor affinity of N_2 on Si with respect to metal-based catalysts; consequently, unmodified SiNWs are unfavorable for N_2 activation and reduction. For instance, Li *et al.*[65] reported that the isoelectric Si heteroatom can only adsorb N_2 through coulomb interaction and consequently resulted in the slightly lengthened N≡N bond of 1.11 Å, which is theoretically unfavorable to the following hydrogenation process for NRR. Our previous theoretical calculations also demonstrate the inferior adsorption ability of N_2 on Si active sites.[66, 67]

In order to improve N_2 affinity on SiNWs, in this work, boron (B), carbon (C) and phosphorus (P) elements have been considered based on their strong capacity to activate N_2 and then reduce into NH_3, as demonstrated by experimental and theoretical reports.[52, 68-70] Herein, for the first time, we investigated undoped SiNWs and then explored single-atom X-doped SiNWs (X = B, C, and P) for NRR in a theoretical comparison. It is worth to note that B/C/P-doped SiNWs have been successfully used for optoelectronic devices, batteries and supercapacitors.[71-73] The as-designed

pristine and doped SiNW details are shown in the electronic supporting information (ESI) and the corresponding optimized B/C/P-doped SiNWs models (named as B_{3C}, B_{2C}, C_{3C}, C_{2C}, P_{3C} and P_{2C}, respectively) along with calculated bonding energy E_b of relevant heteroatoms are shown in Fig. 1. Such large E_b (> 4.00 eV) indicates that, under ambient conditions, the as-obtained X-doped SiNWs would be stable. As demonstrated below, two-coordinated B-dopants (B_{2C}) exhibit excellent activity towards NRR, featured with an ultra-low overpotential (η) of 0.34 V and strongly suppressed hydrogen evolution reaction (HER). Electronic calculations show that boron-doping can decrease the band gap of SiNWs, which would boost the light absorbance and more efficient generation of photoexcited electrons under the photocatalysis scheme. This research not only enriches the pool of metal-free NRR catalysts and may ultimately contribute to the development of 1D nanowires-based catalysts for artificial nitrogen fixation.

2. Calculation details

Under the framework of the Density Functional Theory (DFT), all spin-polarized calculations were performed using the DMol^3 code to investigate the structural and electronic properties of H-passivated Si nanowires (SiNWs) with or without the heteroatoms doping as well as the activity towards NRR. The electron exchange-correlation functional was described by the generalized gradient approximation (GGA) using the revised Perdew-Burk-Ernzerhof (RPBE). The DFT Semi-core Pseudopots (dspp) pseudopotentials and the double numerical basis sets with polarization functions (DNP) were adopted in all calculations. The real-space global cutoff radius is set to be 5.2 Å. The Grimme's method (DFT-D3) was employed to illustrate the Van Der Waal's (VDW) interactions between the catalysts and adsorbates. A (3×3×1) k-point set within the Monkhorst-Pack scheme was used to sample the Brillouin zone for geometry

optimizations. Besides, the solvation effect on NRR was considered using the COSMO scheme with the H_2O dielectric constant of 78.54.[74] All the geometry optimizations were performed until the energy tolerance, the residual force, and SCF tolerance smaller than 10^{-5} Ha, 0.002 Ha/Å, and 10^{-6} Ha, respectively. Based on the computational hydrogen electrode (CHE) model proposed by Nørskov *et al.*,[27, 75, 76] the free energy calculation of the reaction intermediates at 298.15 K and pH = 0 without the extra potential were conducted as follows:

$$\Delta G = \Delta E_{DFT} + \Delta E_{ZPE} - T\Delta S \qquad \text{(eq. 1)}$$

where ΔE_{DFT}, ΔE_{ZPE}, and ΔS are the differences in the electronic energy (E_{DFT}), zero-point vibration energy (E_{ZPE}), and the entropy (S), respectively. The E_{ZPE} can be obtained from the harmonic frequency analyses, where only the active site (Si/B/C/P) and reaction intermediates (N_xH_y) were taken into account for the calculation of Partial Hessian. The entropy of absorbed intermediates can be negligible compared with the free gas molecules (H_2, N_2 & NH_3). Based on the free-energy change of each elementary step, we can evaluate the catalytic activity of NRR. The limiting potential (U_L) of NRR is calculated based on the equation: $U_L = -\Delta G_{max}/e$, which represents the potential required to eliminate the potential-determining step (PDS). Then the overpotential (η) can be obtained from the equation: $\eta = U_e - U_L$, where U_e is the equilibrium potential of nitrogen reduction (U_e = -0.16 V vs. standard hydrogen electrode).

The adsorption energy (E_{ads}) of N_2 is defined as:

$$E_{ads} = E_{composite} - (E_{catalyst} + E_{N2}) \qquad \text{(eq. 2)}$$

where $E_{composite}$ represents the electronic energy of the optimized N_2-catalysts composites. $E_{catalyst}$ and E_{N2} are the electronic energies of optimized catalysts and isolated N_2, respectively. In addition, the heteroatom binding energy (E_b) in SiNWs was calculated according to the equation:

$$E_b = E_{catalyst} - (E_{atom} + E_r) \qquad \text{(eq. 3)}$$

where E_{atom} and E_r are the energies of a single atom and the remaining part of catalysts without the structural optimization. Note that E_b represents the bond strength of the single atom on SiNWs, displaying the stability of active sites. Moreover, the formation energy (μ_f) of X-doped SiNWs can be performed as:

$$\mu_f = E_{doped} + \mu_{Si} - E_{undoped} - \mu_X \qquad \text{(eq. 4)},$$

where E_{doped} and $E_{undoped}$ represent the energies of X-doped and undoped SiNWs, μ_{Si} represents the atomic energy in the Si unit crystal (cubic, 227#), and μ_X indicats the atomic energy in their stable forms, in detail, μ_B, μ_C and μ_P represent the chemical potentials of the atomic boron in α-boron sheet, atomic carbon in bulk graphite, and atomic phosphorus in white phosphorus (P_4) in bulk phase. One thing should be noted that μ_f can express the relative stability compared to the doped-element atoms in their stable structures (such as boron α-sheet, graphene and phosphorene) and the synthesis possibility of doped structures of SiNWs. The synthesis of X-doped SiNWs structures is closely related to the synthesis process/method. More importantly, B/P-doped SiNWs have been reported for many applications, such as batteries and supercapacitors, indicating they can be available under experimental conditions.

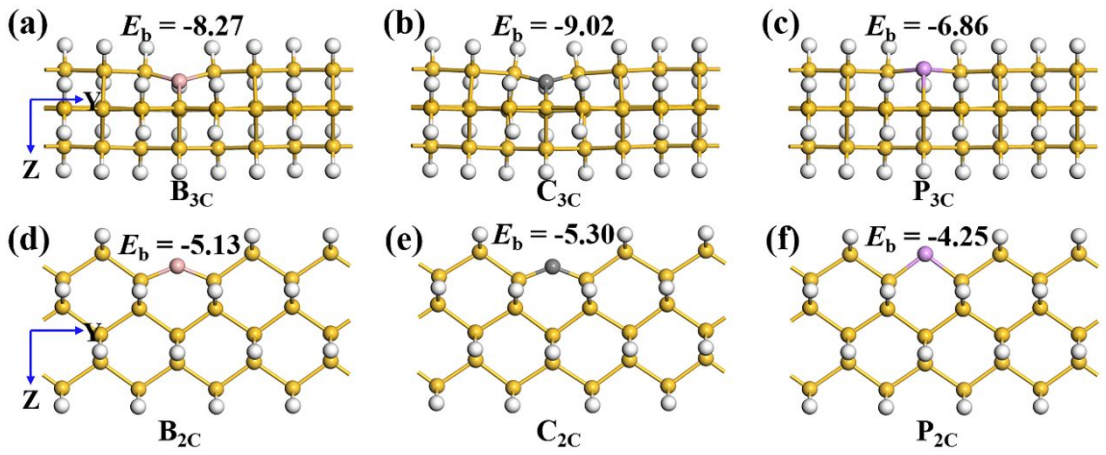

Fig. 1 Doping by p-block elements. The doped SiNWs and their corresponding names (B_{3C}, B_{2C}, C_{3C}, C_{2C}, P_{3C}, and P_{2C}) based on their active sites. E_b is in the unit of eV. Color scheme: Si (yellow), H (White), B (pink), C (grey), P (purple).

3. Results and discussion

3.1. N_2 adsorption and reduction on undoped SiNWs

To examine the speculation of N_2 low affinity over pristine SiNWs and the effect of N_2 adsorption on the whole NRR process, primary calculations of reaction intermediates on Si_{3C} and Si_{2C} were performed first. Generally, there are three associative nitrogen reduction pathways, i.e. distal, alternating and enzymatic ones, by the proton-coupled electron transfer step.[2] The schematic diagram of three NRR schemes is shown in Fig. S3. When N_2 is captured in the end-on mode, NRR can proceed via the distal and alternating pathways; while the enzymatic pathway will only occur beginning from the N_2 side-on adsorption mode on active sites. In the distal pathway, three H^+/e^- pairs first consecutively attack the distal end of absorbed N_2 ($*N_2$) to form the first NH_3 species ($*N_2 \rightarrow *N\text{-}NH \rightarrow *N\text{-}NH_2 \rightarrow *N\text{-}NH_3$). After the release of first NH_3, another three H^+/e^- pairs attack the remaining N-containing species (*N) to synthesize the second

NH_3 (*N → *NH → *NH_2 → *NH_3). In the alternating pathway, six H^+/e^- pairs alternately attack on the *N_2 starting from first attacking the distal N, consequently synthesizing two NH_3 molecules sequentially, through a hydrazine intermediate (*N_2 → *N-NH →*NH-NH → *NH-NH_2 → *NH_2-NH_2 → *NH_2-NH_3 → *NH_3 + NH_3). The NRR process via the enzymatic pathway is quite similar with the alternating one, but the H^+/e^- pairs can simultaneously attack the N adatoms for hydrogenation.

The reaction intermediates on Si_{3C} and Si_{2C} were calculated according to above discussions on NRR mechanisms and the corresponding free energy evolutions, obtained based on the CHE method developed by Nørskov *et al.*,[27] were illustrated in Fig. 2 and Fig. S4-S6 (ESI). Through calculations, we find that the initial N_2 adsorption on SiNWs indeed is energetically unfavorable for the whole NRR process. For instance, up to 1.46 eV energy input is required to stabilize the N_2 adsorption configuration on the Si_{3C} site, as shown in Fig. 2. Critically therefore, NRR would be largely hindered by the initial step. A similar situation has also been observed on Si_{2C} with ΔG_{*N2} = ~0.90 eV (see Fig. S5 and S6). Based on these calculations and the previous work of our group on Si-based catalysts,[66, 67] we propose that active sites with strong N_2 affinity should be introduced for the design of SiNWs-based NRR catalysts. In this context, a doping strategy has been considered to achieve this goal without changing the intrinsic electronic structures of SiNWs.[77-80] Here, low-cost p-block elements (B, C, and P) were doped to occupy Si_{3C} and Si_{2C} sites, as shown in Fig. 1. More characteristics about doped SiNWs are shown in Table S1. Carbon comes from the same group as silicon, which does not introduce additional valence electrons or holes, but boron and phosphorus will result in hole- and electron-doping due to their

different electronic configurations. Such investigation can help us to establish advanced understanding on the doping effect.

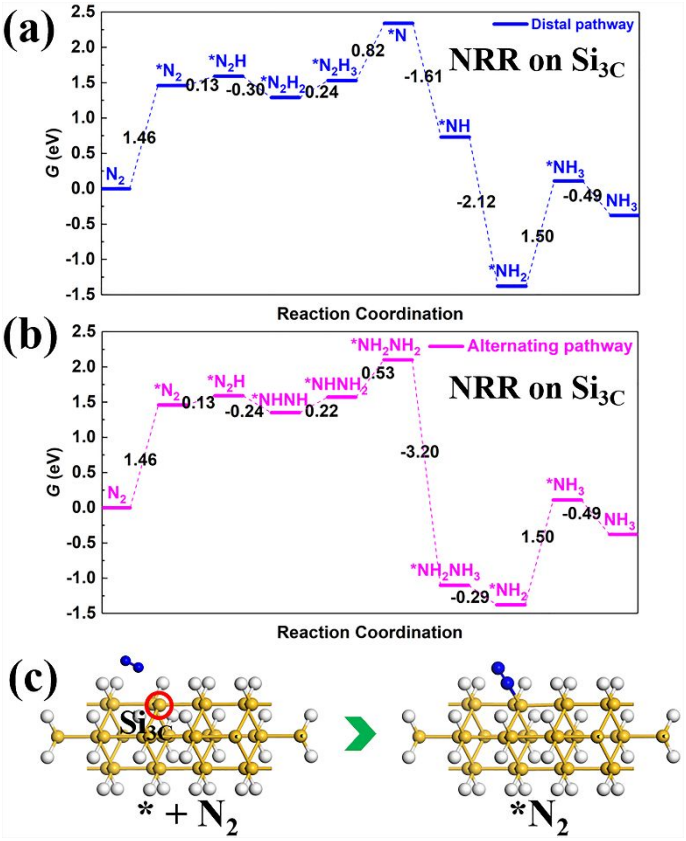

Fig. 2 (a, b) Diagram of the free energy evolution along the reaction coordination for distal and alternating pathways, and (c) N_2 capture on Si_{3C}. Color scheme: Si (yellow), H (White), N (blue).

3.2. N_2 adsorption on doped SiNWs

Dinitrogen adsorption is the initial step of NRR, which determines the following N_2 reduction process. Fig. 3 displays the differently local adsorption configurations of N_2 over single-atom B-, C- and P-doped SiNWs, with three potential geometries over each dopant. Dinitrogen adsorption configurations in different perspectives are shown in Fig. S7. Adsorption energies (E_{ads}) and free-energy changes (ΔG) upon the adsorption of N_2 on dopants are shown in Fig. 3, in which we

can notice that B- and C-doped SiNWs exhibit significant improvement on N_2 adsorption with larger E_{ads} (see Fig. 3a-3f), while in Fig. 3g and 3h, the N_2 adsorption on P_{3C} and P_{2C} shows weak physisorption with small E_{ads} of merely -0.06 and -0.05 eV and the unchanged N-N bond length of $*N_2$ with 1.11 Å; and N_2 side-on adsorption configuration on the P_{2C} site is relatively unstable due to the largely positive E_{ads} (2.63 eV) and ΔG (3.16 eV) from the view of energy, as shown in Fig. 3i. This indicates that NRR would not occur on P-doped SiNWs. As a result, in our following discussions, we will just focus on N_2 capture and activation on single-atom B- and C-doped SiNWs.

We can see from Fig. 3a-3c, that the N_2 can be adsorbed on the B active site with E_{ads} ranging from -0.13 to -1.48 eV, suggesting the strong interaction between N_2 and B active sites. Taking the Zero Point Energy (ZPE) and entropy into account for the free-energy correction, we can find the adsorption on B_{3C} and B_{2C} would be spontaneous, while N_2 would prefer to absorb on the B_{2C} site in the end-on pattern with ΔG_{*N2} = -0.87 eV (Fig. 3b). Likewise, based on the energy analysis of N_2 adsorption on C_{3C} and C_{2C} sites shown in Fig. 3d-3f, one can calculate a physisorption interaction between N_2 and C_{3C} with small E_{ads} of -0.08 eV, which suggests that N_2 would not be well-activated in this way. The unchanged N-N bond length of 1.11 Å provides further evidence that NRR will not likely occur on C_{3C}; however, N_2 could be spontaneously captured on C_{2C} in the end-on (vertical) and side-on (horizontal) modes with negative free-energy values of -1.26 and -0.06 eV. In these cases, the triple bond of N_2 on C_{2C} is activated and elongated to 1.16 and 1.23 Å, respectively. Based on the above analysis on N_2 adsorption, in the following discussion on the NRR process, the end-on adsorption configurations on B_{3C}, B_{2C} and

both the end-on and side-on adsorption configurations on C_{2C} are taking as the starting points for the subsequent hydrogenation process.

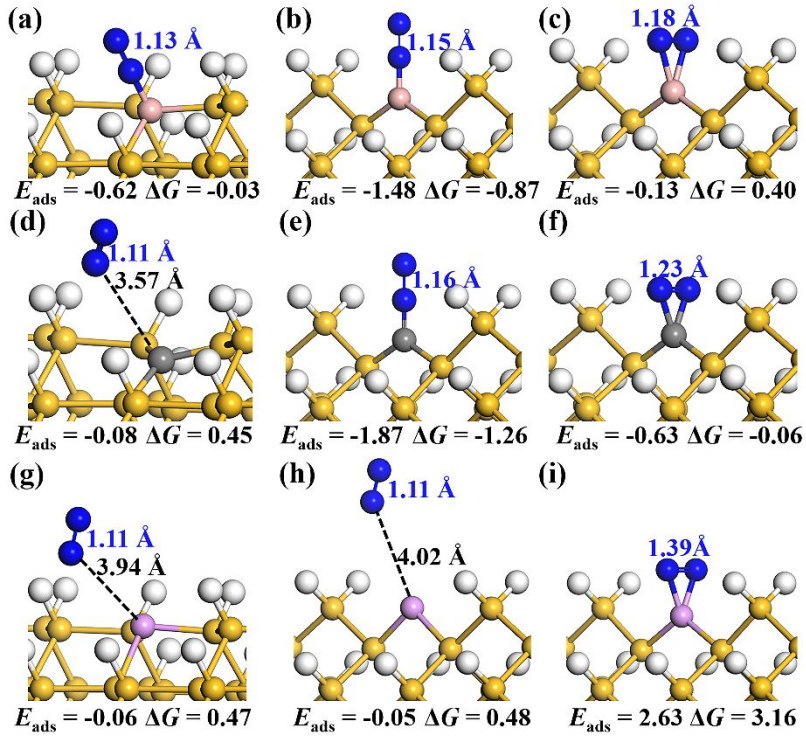

Fig. 3 Local adsorption configurations of N_2 on B-doped (a-c), C-doped (d-f), P-doped (g-i) SiNWs along with the energy changes. Both E_{ads} and ΔG are in the unit of eV. Black values near the dash line indicate the distance between N_2 and active sites. Blue values show the N-N bond length of $*N_2$ on doped SiNWs. Color scheme: Si (yellow), H (White), N (blue), B (pink), C (grey) and P (purple).

3.3. N_2 reduction on C-doped SiNWs

Since carbon and silicon have the similar valence structures (in the same IV A column), we will first discuss the effect of C-doping on NRR. Based on the above-mentioned energetically favorable adsorption configurations of N_2 on C_{2C}, in end-on and side-on orientation, there are three associative nitrogen reduction pathways. Therefore, based on the distal, alternating and

enzymatic reaction pathways proposed, NRR intermediates on C_{2C} were investigated and the corresponding relevant free-energy evolution was calculated according to the CHE method. Here, it should note that the ΔG_{max} should come from the hydrogenation or the proton-coupled electron transfer step, not the release of NH_3, because the formed NH_3 can be easily converted into the form of NH_4^+ in acidic electrolytes and desorb from active sites smoothly according to relevant reports.[81] Thus, NH_3 release is not a problematic issue to consider in an acidic environment. Fig. 4 demonstrates the free-energy evolution of NRR on C_{2C} and the corresponding NRR intermediates ($*N_xH_y$) are shown in Fig. S8. From Fig. 4, one can notice that the first hydrogenation ($*N_2 + H^+ + e^- \rightarrow *N_2H$) of all NRR pathways on C_{2C} is the potential-determining step (PDS) with $\Delta G_{max} > 1.00$ eV, which indicates that NRR activity would be limited due to such large free-energy changes. Therefore, C-introducing into SiNWs cannot largely boost the NRR performance although N_2 adsorption is improved.

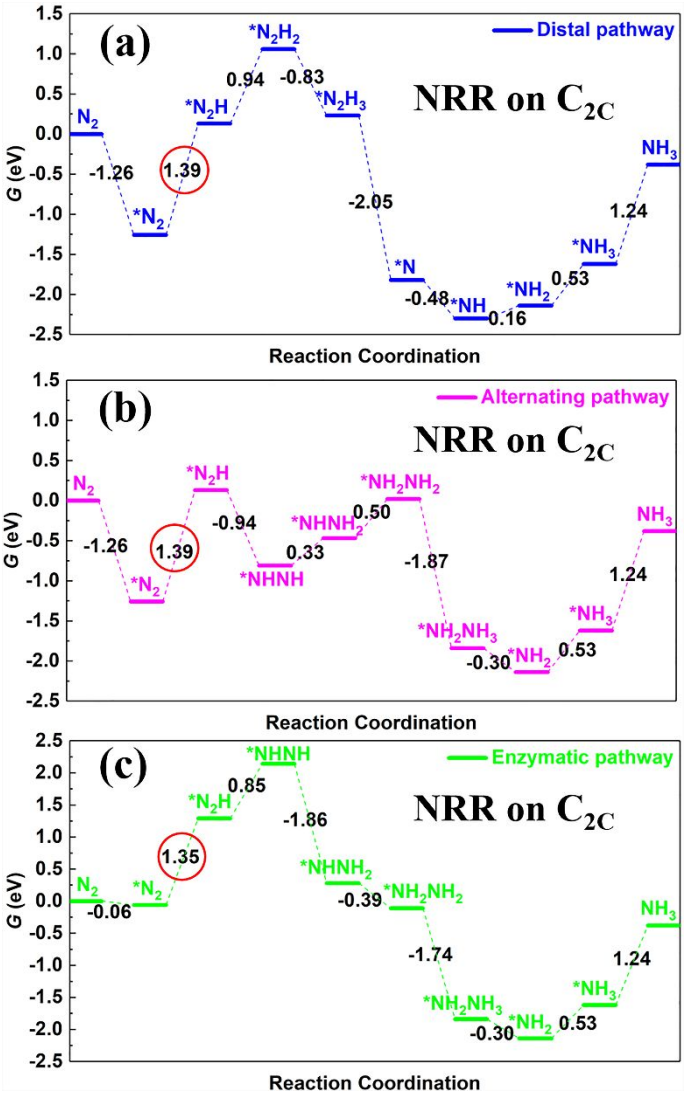

Fig. 4 Free-energy evolution of NRR on C_{2C} along distal (a), alternating (b), and enzymatic (c) pathways. The values of free energy changes are in the unit of eV.

3.4. N_2 reduction on B-doped SiNWs

Fig. 5 exhibits the free-energy evolution of NRR on B_{3C} and B_{2C} along the reaction coordination through the distal and alternating pathways. Their corresponding NRR intermediates ($*N_xH_y$) are shown in Fig. S9-S10 and Fig. 6a. From Fig. 5a and 5b, we can notice that the maximum free-

energy change on B_{3C} occurs also from the first hydrogenation step ($*N_2 + H^+ + e^- \rightarrow *N_2H$) with the limiting potential (U_L) of -1.88 V (η = 1.72 V) for both distal and alternating reaction pathways, which means NRR activity will be severely limited by the first hydrogenation step due to the considerably unfavourable free-energy change. However, in Fig. 5c, the maximum free-energy change on B_{2C} through the distal pathway is mere 0.50 eV, which comes from the second hydrogenation step ($*N_2H + H^+ + e^- \rightarrow *N_2H_2$). Furthermore, compared with the maximum free-energy change (1.56 eV) of $*NHNH_2 + H^+ + e^- \rightarrow *NH_2NH_2$ via the alternating pathway (see Fig. 5d), we calculate that the optimal NRR process on B_{2C} is the distal pathway with the low U_L and η of -0.50 and 0.34 V, respectively. From this we can conclude that B_{2C} exhibits the highest performance towards NRR with the lowest η of 0.34 V, which theoretically outperforms some recently reported metal-free catalysts[66, 69, 82] and even some metal single-atom catalysts (SACs), like BN/V/G sandwiched structure (U_L = -0.89 V, η = 0.73 V),[43] MoN_4 (U_L = -0.67 V, η = 0.51 V).[83] More comparison on theoretical U_L and η was summarized in ESI (see Table S2).

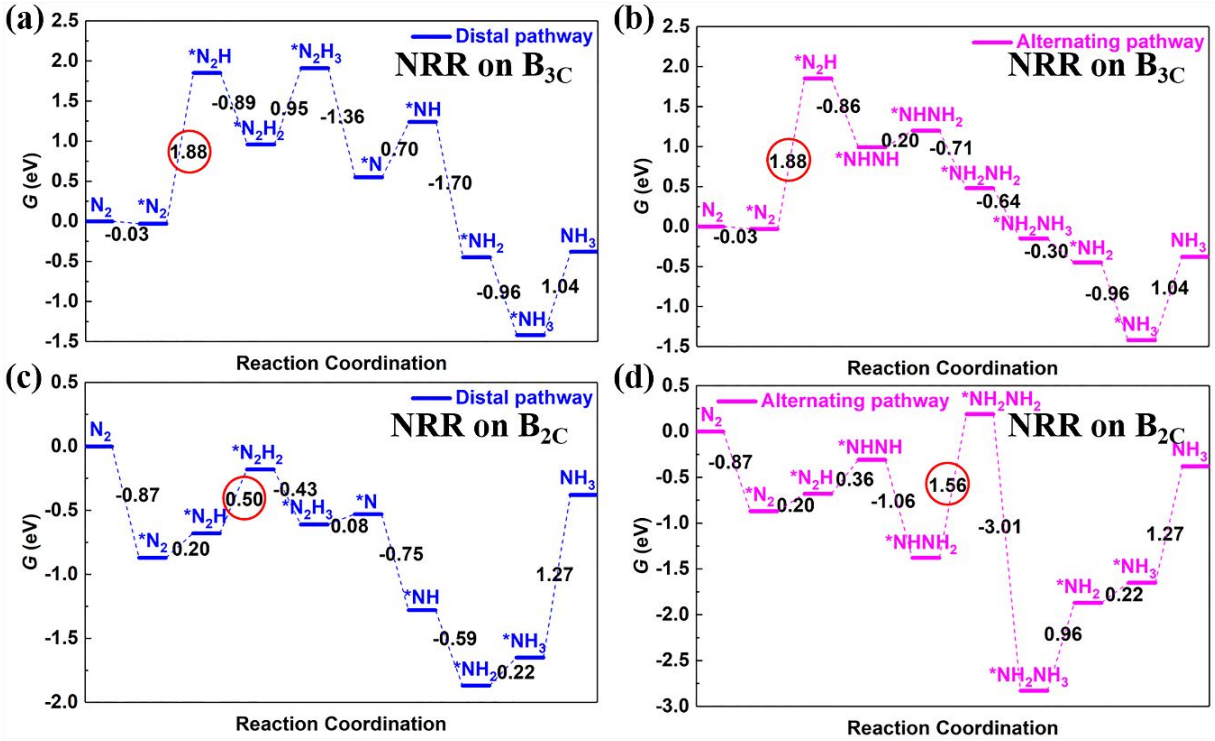

Fig. 5 Free-energy diagram of NRR on B_{3C} (a, b) and B_{2C} (c, d). The values of free energy changes are in the unit of eV.

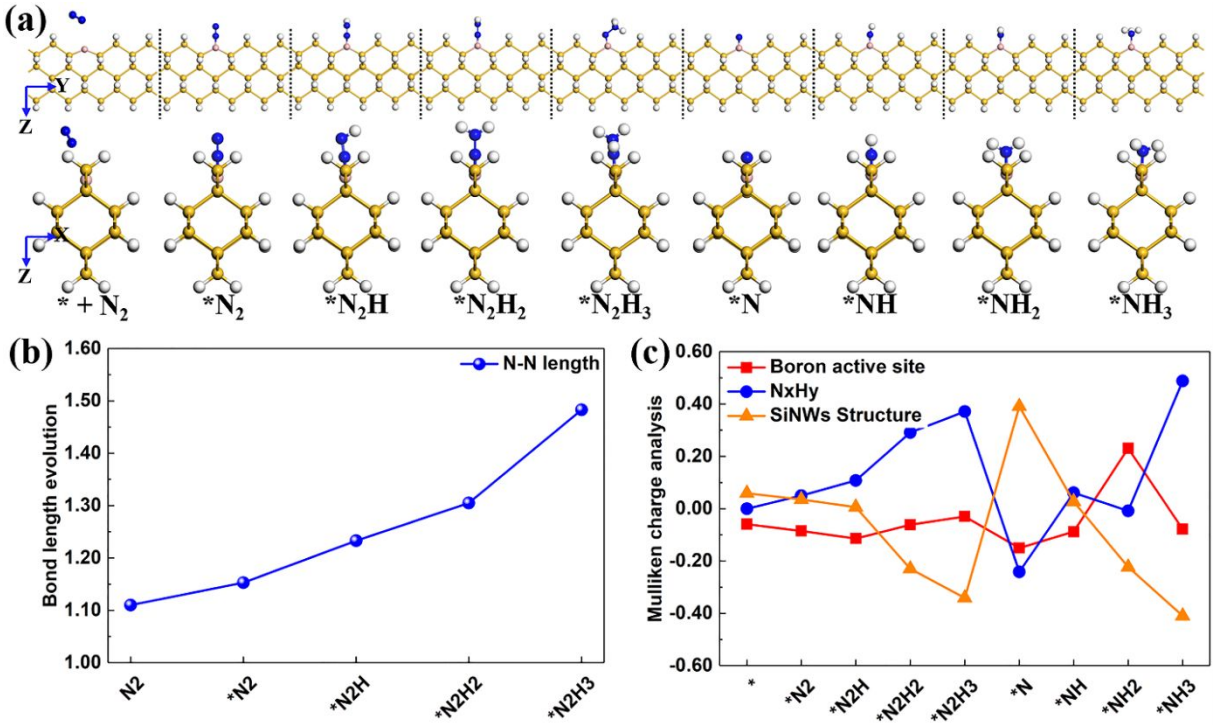

Fig. 6 (a) NRR intermediates on B_{2C} along the distal pathway; (b) N-N bond length evolution before the release of first NH_3; (c) Mulliken charges analysis of three moieties, including boron active site, N_xH_y species, and SiNWs structure, along the reaction coordination.

With B_{2C} described as the best catalyst candidate, Fig. 6a displays the NRR intermediates of the optimal distal pathway. Fig. 6b shows the corresponding evolution of N-N bond length of reaction intermediates ($*N_xH_y$), where it can be seen that the N-N bond elongates steadily bit by bit from initial 1.11 Å (free N_2 molecule) to 1.48 Å till the release of the first NH_3 molecule, which suggests that the N-N bond is weakened, bit by bit, by hydrogenation steps. Such a gradual elongation on the N-N bond will be helpful to avoid the large fluctuation of the free-energy evolution and explains, in a way, why B_{2C} is suitable for NRR. In addition, the charge analysis along the NRR distal pathway was performed and shown in Fig. 6c (Mulliken charge) and Fig. S11 (Hirshfeld charge). Mulliken and Hirshfeld charge analysis exhibits a similar trend although their absolute values are different. Here, we divided reaction intermediates into three moieties: adsorbed species (moiety 1: N_xH_y), B active site (moiety 2), and the SiNW structure (moiety 3). In Fig. 6c, we can notice that the charge change trend of N_xH_y is contrary to that of SiNW roughly and the charge prefers to transfer from N_xH_y to SiNW when hydrogenation occurs. Moreover, the charge on the B_{2C} active site oscillates during the whole process of NRR, which indicates that the active site could also contribute to the charges of N_xH_y to some degree. Therefore, during the process of NRR, the SiNW structure mainly acts as the electron reservoir and the B active site mainly plays the crucial role of transferring electron density back and forth between SiNW and N_xH_y and also mediates the charges of N_xH_y as the NRR progresses.

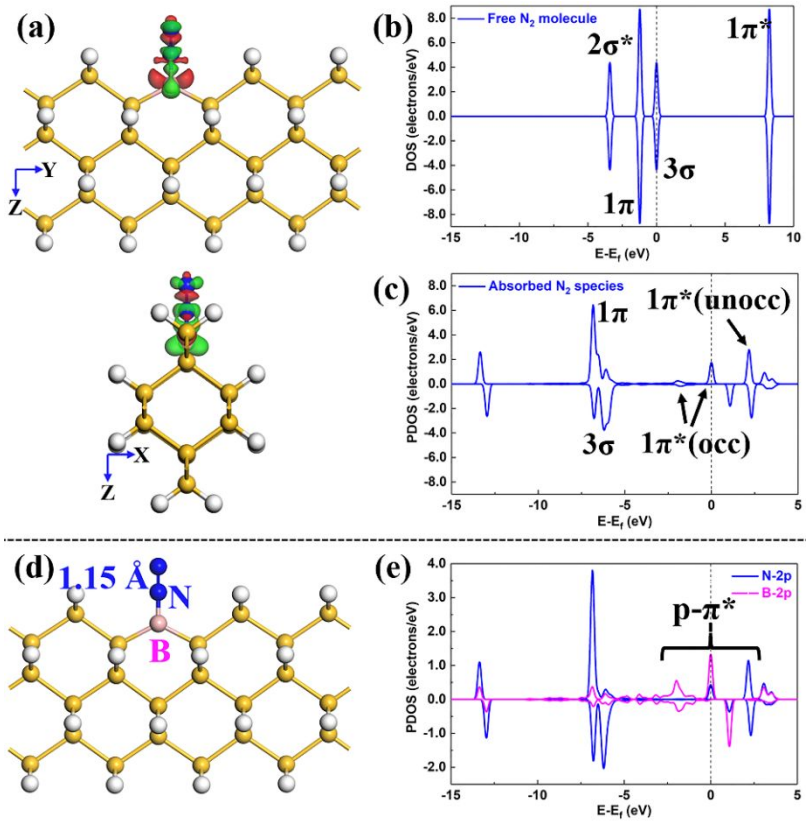

Fig. 7 (a) Electron density difference analysis of $*N_2$ on B_{2C}, in which green and red represent the electron accumulation and loss region, respectively (isosurface: 0.05 a.u.); (b, c) Density of States (DOS) analysis before and after the adsorption of N_2 on B_{2C}; (d, e) the schematic diagram of both N and B atoms and their corresponding DOS analysis to indicate their *p*-orbital interactions. Note that "unocc" and "occ" represent the unoccupied and occupied states of 1π* orbital of dinitrogen, respectively.

In order to investigate the origin of NRR activity on B_{2C}, the electron density difference of $*N_2$ was calculated as shown in Fig. 7a. Obviously, the two-way electron transfer between the B site and adsorbed $*N_2$ has occurred, i.e. acceptance-donation process, due to the electron loss and accumulation around B and absorbed $*N_2$.[52, 68, 82, 84] The active B accepts the electrons of N_2

(Lewis base), and simultaneously donates its electron to the antibonding ($1\pi^*$) of N-N bond. The elongated N-N bond (1.15 Å) and decreased electron density of N-N bond (see Fig. 7a) suggest that the stable N≡N is well-activated on B_{2C}. From Fig. 7b and 7c, we can notice that the adsorbed $*N_2$ has been spin-polarized resulted from the B interaction with the π and 3σ orbital of $*N_2$. Furthermore, in Fig. 7d and 7e, it can be noticed that there is a discernible overlap around the Fermi level between B-2*p* and N-2*p* orbitals, indicating their strong interaction. This well-activated $*N_2$ is mainly due to the high-spin ground state of the active B_{2C} site in SiNWs, which is reported to be conducive to active stable N_2.[85]

3.5. HER

HER is a competing side reaction during NRR, which can reduce the selectivity of converting N_2 into NH_3. Therefore, both HER and NRR activities should both be considered for NRR catalyst design. As the side reaction during the process of NRR, the HER not only decreases the FE, but also the adsorption of H can block active sites, where the NRR initiates. We therefore first analyzed the adsorption selectivity of N_2 and H on the active site. From Fig. 4 and Fig. 5, we can see $\Delta G(*N_2)$ on C_{2C}, B_{3C}, and B_{2C} are -1.26 (-0.06), -0.03, and -0.87 eV, respectively, while the corresponding $\Delta G(*H)$ are -1.59, +0.35, and -0.86 eV in Fig. 8a. Based on the differences between $\Delta G(*N_2)$ and $\Delta G(*H)$ on these three active sites, one can deduce that on B_{3C} and B_{2C}, the adsorption of N_2 has a competitive ability over the adsorption of H and thus HER will be hindered by the Volmer step ($* + H^+ + e^- \rightarrow *H$), which is helpful to improve the selectivity of NRR, while the adsorption of H will dominate over N_2 adsorption on C_{2C}. Then, as shown in Fig. 8b, we compared the difference between the maximum free-energy changes on the PDS of NRR (ΔG_{max}^{NRR}) and HER (ΔG_{max}^{HER}). Based on the maximum free-energy changes of HER and

NRR on C_{2C}, B_{3C}, and B_{2C} and (see Fig. 8b), one can deduce that B_{2C} and C_{2C} would have decent NRR selectivity due to less energy requirements for NRR. HER will be effectively hindered by the Heyrovskey step ($*H + H^+ + e^- \rightarrow H_2$) on B_{2C} and C_{2C} due to the large adsorption free-energies of *H. Importantly, among catalysts investigated, B_{2C} exhibits the highest activity towards NRR with the maximum free-energy change of mere 0.50 eV (U_L = -0.50 V). Therefore, following the work of Li and coworkers,[86] the selectivity of NH_3 production on B_{2C} was further estimated based on the Boltzmann distribution:

$$f_{NRR} = 1/(1 + \exp\left[\left(\Delta G_{PDS}(NRR) - \Delta G_{PDS}(HER)\right)/k_B T\right])$$

where ΔG_{PDS} is the Gibbs free-energy change on PDS, k_B is the Boltzmann constant, and T is the temperature and set to 298.15 K here. f_{NRR} is the approximation of the mole fraction of NH_3 in the total products (NH_3 + H_2). According to this equation (f_{NRR}), the NRR selectivity on B_{2C} would almost be ~100% under ambient conditions with the assumption that the NRR and HER are rate-controlled only by their PDS. As a result, B_{2C} holds a great promising prospect to realize NRR as a photocatalyst with an expectant excellent selectivity. To explore band-gap implications, we performed the band structure calculations of both pristine and single-atom B-doped SiNW (B_{2C}) with the hybrid functional of Heyd-Scuseria-Ernzerhof (HSE06) and found that the band gap is reduced from 2.04 eV to 0.72 eV when the single-atom B was doped into the Si_{2C} site (shown in Fig. S12), which is mainly due to the introduction of impurity level. This largely decreased band gap indicates that the electrical conductivity and electron transfer for NRR are enhanced, and importantly, the light absorbance of B_{2C} would be distinctly improved. As a photocatalyst, B_{2C} would have an excellent ability for generating photo-excited electrons and then efficient photocatalytic NRR performance.

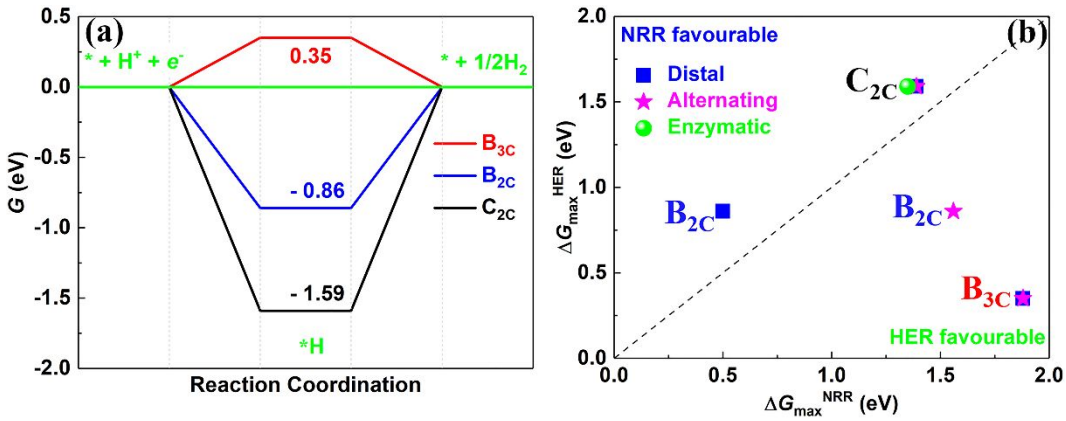

Fig. 8 HER performance analysis. (a) HER diagram of free energy evolution along the reaction coordination; (b) NRR selectivity analysis with ΔG_{max}^{NRR} *vs.* ΔG_{max}^{HER}.

As the best catalyst, B_{2C} was further investigated for its formation energy (μ_f) (see eq. 4), we calculated that μ_f was 0.28 eV, which makes B_{2C} quite feasible to be synthesized under ambient conditions experimentally - the μ_f values of other doped SiNWs were shown in Table S1. More importantly, the growth route of pure and doped SiNWs are facile and available, because presently *n*-type and *p*-type doped SiNWs have been experimentally reported for energy conversion,[71, 79] such as P-/B-doped SiNWs. Therefore, this work can take great advantage of current development on SiNWs for photocatalytic nitrogen fixation. In addition, by the integration with some conductive materials via self-assembly techniques,[62, 87-90] B-doped SiNWs (B_{2C}) holds a promising prospect to act as a (photo)electrocatalyst for NRR.

4. Conclusion

In summary, p-block element-doped SiNWs have addressed the problem of capture and activation of N_2 on the Si site. Among investigated models, single-atom B-doping (*p*-type) in the two-coordinated position (B_{2C}) has exhibited very exciting activity towards photocatalytic NRR

due to the ultra-low overpotential of 0.34 V, suppressed HER performance, high-spin ground state of the B active site, and decreased band gap for enhancing light absorbance and therefore more efficient generation of photo-excited electrons. This work not only uses heteroatom-doping to activate the SiNWs, and enriches the pool of NRR catalysts, but also boosts the investigation of 1D nanomaterials for realizing artificial nitrogen fixation.

ASSOCIATED CONTENT

Electronic Supporting information (ESI): calculation details, catalyst model details, and other relevant calculation data.

AUTHOR INFORMATION

Corresponding authors:

Siyao Qiu - School of Chemical Engineering and Energy Technology, Dongguan University of Technology, Dongguan 523808, China; Email: qiusy@dgut.edu.cn

Chenghua Sun - Department of Chemistry and Biotechnology, Centre for Translational Atomaterials, Swinburne University of Technology, Hawthorn, Victoria 3122, Australia; Email: chenghuasun@swin.edu.au

Conflicts of interest

There are no conflicts to declare.

ACKNOWLEDGMENTS

The authors acknowledge the financial support by Guangdong Innovation Research Team for Higher Education (2017KCXTD030), High-level Talents Project of Dongguan University of

Technology (KCYKYQD2017017), Engineering Research Center of None-food Biomass Efficient Pyrolysis and Utilization Technology of Guangdong Higher Education Institutes (2016GCZX009) and Research Center of New Energy Materials (KCYCXPT2017005). The authors also thank the National Computational Infrastructure (NCI), which is supported by the Australian Government, for providing the computational resources.

REFERENCES

1. V. Smil, *Nature*, 1999, **400**, 415-415.
2. S. L. Foster, S. I. P. Bakovic, R. D. Duda, S. Maheshwari, R. D. Milton, S. D. Minteer, M. J. Janik, J. N. Renner and L. F. Greenlee, *Nat. Catal.*, 2018, **1**, 490-500.
3. J. W. Erisman, M. A. Sutton, J. Galloway, Z. Klimont and W. Winiwarter, *Nat. Geosci.*, 2008, **1**, 636-639.
4. V. Smil, *World Agric.*, 2011, **2**, 9-13.
5. R. D. Milton, S. Abdellaoui, N. Khadka, D. R. Dean, D. Leech, L. C. Seefeldt and S. D. Minteer, *Energy Environ. Sci.*, 2016, **9**, 2550-2554.
6. J. Christiansen, D. R. Dean and L. C. Seefeldt, *Annu. Rev. Plant Physiol. Plant Mol. Biol.*, 2001, **52**, 269-295.
7. K. A. Brown, D. F. Harris, M. B. Wilker, A. Rasmussen, N. Khadka, H. Hamby, S. Keable, G. Dukovic, J. W. Peters, L. C. Seefeldt and P. W. King, *Science*, 2016, **352**, 448-450.
8. J. G. Chen, R. M. Crooks, L. C. Seefeldt, K. L. Bren, R. M. Bullock, M. Y. Darensbourg, P. L. Holland, B. Hoffman, M. J. Janik, A. K. Jones, M. G. Kanatzidis, P. King, K. M. Lancaster, S. V. Lymar, P. Pfromm, W. F. Schneider and R. R. Schrock, *Science*, 2018, **360**, eaar6611.
9. C. J. M. van der Ham, M. T. M. Koper and D. G. H. Hetterscheid, *Chem. Soc. Rev.*, 2014, **43**, 5183-5191.
10. V. Kyriakou, I. Garagounis, A. Vourros, E. Vasileiou and M. Stoukides, *Joule*, 2020, **4**, 142-158.

11. G. Hochman, A. S. Goldman, F. A. Felder, J. M. Mayer, A. J. M. Miller, P. L. Holland, L. A. Goldman, P. Manocha, Z. Song and S. Aleti, *ACS Sustainable Chem. Eng.*, 2020, **8**, 8938-8948.

12. S. Licht, B. Cui, B. Wang, F.-F. Li, J. Lau and S. Liu, *Science*, 2014, **345**, 637-640.

13. H. Liu, *Chin. J. Catal.*, 2014, **35**, 1619-1640.

14. Y. Sun, Z. Deng, X.-M. Song, H. Li, Z. Huang, Q. Zhao, D. Feng, W. Zhang, Z. Liu and T. Ma, *Nano-Micro Lett.*, 2020, **12**, 133.

15. K. Ithisuphalap, H. Zhang, L. Guo, Q. Yang, H. Yang and G. Wu, *Small Methods*, 2019, **3**, 1800352.

16. X. Yang, S. Zhou, S. Huang and J. Zhao, *J. Phys. Chem. C*, 2020, **124**, 23798-23806.

17. H. Zou, W. Rong, S. Wei, Y. Ji and L. Duan, *Proc. Natl. Acad. Sci.*, 2020, **117**, 29462-29468.

18. J. Pan, H. A. Hansen and T. Vegge, *J. Mater. Chem. A*, 2020, **8**, 24098-24107.

19. X. Guo, S. Lin, J. Gu, S. Zhang, Z. Chen and S. Huang, *Adv. Funct. Mater.*, 2021, **31**, 2008056.

20. X. Niu, Q. Zhu, S. Jiang and Q. Zhang, *J. Phys. Chem. Lett.*, 2020, **11**, 9579-9586.

21. W. Zhang, J. Low, R. Long and Y. Xiong, *EnergyChem*, 2020, **2**, 100040.

22. Y. Li, Y. Fang, Y. Xue, L. Hui and H. Yu, *Angew. Chem. Int. Ed.*, 2020, **60**, 3170-3174.

23. S. Z. Andersen, M. J. Statt, V. J. Bukas, S. G. Shapel, J. B. Pedersen, K. Krempl, M. Saccoccio, D. Chakraborty, J. Kibsgaard, P. C. K. Vesborg, J. Nørskov and I. Chorkendorff, *Energy Environ. Sci.*, 2020, **13**, 4291-4300.

24. C. Guo, J. Ran, A. Vasileff and S.-Z. Qiao, *Energy Environ. Sci.*, 2018, **11**, 45-56.

25. Y. Liu, P. Deng, R. Wu, X. Zhang, C. Sun and H. Li, *J. Mater. Chem. A*, 2021, DOI: 10.1039/D0TA11522C.

26. X. Chen, N. Li, Z. Kong, W.-J. Ong and X. Zhao, *Mater. Horiz.*, 2018, **5**, 9-27.

27. E. Skúlason, T. Bligaard, S. Gudmundsdóttir, F. Studt, J. Rossmeisl, F. Abild-Pedersen, T. Vegge, H. Jónsson and J. K. Nørskov, *Phys. Chem. Chem. Phys.*, 2012, **14**, 1235-1245.

28. Á. Logadóttir and J. K. Nørskov, *J. Catal.*, 2003, **220**, 273-279.

29. J. H. Montoya, C. Tsai, A. Vojvodic and J. K. Nørskov, *ChemSusChem*, 2015, **8**, 2180-2186.

30. L. M. Azofra, N. Li, D. R. MacFarlane and C. Sun, *Energy Environ. Sci.*, 2016, **9**, 2545-2549.

31. S. Zhang, M. Jin, T. Shi, M. Han, Q. Sun, Y. Lin, Z. Ding, L. R. Zheng, G. Wang, Y. Zhang, H. Zhang and H. Zhao, *Angew. Chem. Int. Ed.*, 2020, **59**, 13423-13429.

32. J. Zhao and Z. Chen, *J. Am. Chem. Soc.*, 2017, **139**, 12480-12487.

33. M. I. Ahmed, S. Chen, W. Ren, X. Chen and C. Zhao, *Chem. Commun.*, 2019, **55**, 12184-12187.

34. H.-B. Wang, J.-Q. Wang, R. Zhang, C.-Q. Cheng, K.-W. Qiu, Y.-j. Yang, J. Mao, H. Liu, M. Du, C.-K. Dong and X.-W. Du, *ACS Catal.*, 2020, **10**, 4914-4921.

35. L. J. Arachchige, Y. Xu, Z. Dai, X. L. Zhang, F. Wang and C. Sun, *J. Mater. Sci. Technol.*, 2021, **77**, 244-251.

36. L. Jasin Arachchige, Y. Xu, Z. Dai, X. Zhang, F. Wang and C. Sun, *J. Phys. Chem. C*, 2020, **124**, 15295-15301.

37. Q. Li, L. He, C. Sun and X. Zhang, *J. Phys. Chem. C*, 2017, **121**, 27563-27568.

38. C. Liu, Q. Li, J. Zhang, Y. Jin, D. R. MacFarlane and C. Sun, *J. Mater. Chem. A*, 2019, **7**, 4771-4776.

39. B. Ma, H. Zhao, T. Li, Q. Liu, Y. Luo, C. Li, S. Lu, A. M. Asiri, D. Ma and X. Sun, *Nano Res.*, 2020, **14**, 555-569.

40. J. Zhang, B. Zhao, W. Liang, G. Zhou, Z. Liang, Y. Wang, J. Qu, Y. Sun and L. Jiang, *Adv. Sci.*, 2020, **7**, 2002630.

41. S. Zhang, Y. Zhao, R. Shi, C. Zhou, G. I. N. Waterhouse, Z. Wang, Y. Weng and T. Zhang, *Angew. Chem. Int. Ed.*, 2020, **60**, 2554-2560.

42. L.-F. Gao, Y. Cao, C. Wang, X.-W. Yu, W.-B. Li, Y. Zhou, B. Wang, Y. Yao, C.-P. Wu, W.-J. Luo and Z.-G. Zou, *Angew. Chem. Int. Ed.*, 2020, **60**, 5257-5261.

43. S. Tang, Q. Dang, T. Liu, S. Zhang, Z. Zhou, X. Li, X. Wang, E. Sharman, Y. Luo and J. Jiang, *J. Am. Chem. Soc.*, 2020, **142**, 19308-19315.

44. X. Chen, X. Zhao, Z. Kong, W.-J. Ong and N. Li, *J. Mater. Chem. A*, 2018, **6**, 21941-21948.

45. A. R. Singh, B. A. Rohr, J. A. Schwalbe, M. Cargnello, K. Chan, T. F. Jaramillo, I. Chorkendorff and J. K. Nørskov, *ACS Catal.*, 2016, **7**, 706-709.

46. B. H. R. Suryanto, H.-L. Du, D. Wang, J. Chen, A. N. Simonov and D. R. MacFarlane, *Nat. Catal.*, 2019, **2**, 290-296.

47. E. Skúlason, T. Bligaard, S. Gudmundsdóttir, F. Studt, J. Rossmeisl, F. Abild-Pedersen, T. Vegge, H. Jónsson and J. K. Nørskov, *Phys. Chem. Chem. Phys.*, 2012, **14**, 1235-1245.

48. S. Zhao, X. Lu, L. Wang, J. Gale and R. Amal, *Adv. Mater.*, 2019, **31**, 1805367.

49. Y. Huang, D. D. Babu, Z. Peng and Y. Wang, *Adv. Sci.*, 2020, **7**, 1902390.

50. Y. Tian, D. Xu, K. Chu, Z. Wei and W. Liu, *J. Mater. Sci.*, 2019, **54**, 9088-9097.

51. H. Li, L. Yang, Z. Wang, P. Jin, J. Zhao and Z. Chen, *J. Energy Chem.*, 2020, **46**, 78-86.

52. X. Yu, P. Han, Z. Wei, L. Huang, Z. Gu, S. Peng, J. Ma and G. Zheng, *Joule*, 2018, **2**, 1610-1622.

53. Y. Liu, Y. Su, X. Quan, X. Fan, S. Chen, H. Yu, H. Zhao, Y. Zhang and J. Zhao, *ACS Catal.*, 2018, **8**, 1186-1191.

54. S. Mukherjee, D. A. Cullen, S. Karakalos, K. Liu, H. Zhang, S. Zhao, H. Xu, K. L. More, G. Wang and G. Wu, *Nano Energy*, 2018, **48**, 217-226.

55. C. Zhao, S. Zhang, M. Han, X. Zhang, Y. Liu, W. Li, C. Chen, G. Wang, H. Zhang and H. Zhao, *ACS Energy Lett.*, 2019, **4**, 377-383.

56. L. Zhang, L.-X. Ding, G.-F. Chen, X. Yang and H. Wang, *Angew. Chem. Int. Ed.*, 2019, **58**, 2612-2616.

57. B. Liu and K. Zhou, *Prog. Mater Sci.*, 2019, **100**, 99-169.

58. Y. Jia, J. Chen and X. Yao, *Mater. Chem. Front.*, 2018, **2**, 1250-1268.

59. C. Lv, Y. Qian, C. Yan, Y. Ding, Y. Liu, G. Chen and G. Yu, *Angew. Chem. Int. Ed. Engl.*, 2018, **57**, 10246-10250.

60. D. R. MacFarlane, P. V. Cherepanov, J. Choi, B. H. R. Suryanto, R. Y. Hodgetts, J. M. Bakker, F. M. Ferrero Vallana and A. N. Simonov, *Joule*, 2020, **4**, 1186-1205.

61. V. Schmidt, J. V. Wittemann and U. Gösele, *Chem. Rev.*, 2010, **110**, 361-388.

62. A. I. Hochbaum and P. Yang, *Chem. Rev.*, 2010, **110**, 527-546.

63. Y. Wang, T. Wang, P. Da, M. Xu, H. Wu and G. Zheng, *Adv. Mater.*, 2013, **25**, 5177-5195.

64. E. L. Warren, H. A. Atwater and N. S. Lewis, *J. Phys. Chem. C*, 2013, **118**, 747-759.

65. G.-Y. Zhai, D. Xu, S.-N. Zhang, Z.-H. Xue, H. Su, Q.-Y. Yu, H.-H. Wang, X. Lin, Y.-X. Lin, L.-H. Sun, X.-H. Li and J.-S. Chen, *Adv. Funct. Mater.*, 2020, **30**, 2005779.

66. Z. Guo, S. Qiu, H. Li, Y. Xu, S. J. Langford and C. Sun, *Phys. Chem. Chem. Phys.*, 2020, **22**, 21761-21767.

67. Z. Guo, S. Qiu, H. Li, Y. Xu, S. J. Langford and C. Sun, *ChemCatChem*, 2021, **13**, 1239-1245.

68. C. Liu, Q. Li, C. Wu, J. Zhang, Y. Jin, D. R. MacFarlane and C. Sun, *J. Am. Chem. Soc.*, 2019, **141**, 2884-2888.

69. Z. Guo, S. Qiu, H. Li, Y. Xu, S. J. Langford and C. Sun, *Diamond Relat. Mater.*, 2021, **111**, 108210.

70. L. Zhang, L. X. Ding, G. F. Chen, X. Yang and H. Wang, *Angew. Chem. Int. Ed. Engl.*, 2019, **58**, 2612-2616.

71. O. Burchak, C. Keller, G. Lapertot, M. Salaün, J. Danet, Y. Chen, N. Bendiab, B. Pépin-Donat, C. Lombard, J. Faure-Vincent, A. Vignon, D. Aradilla, P. Reiss and P. Chenevier, *Nanoscale*, 2019, **11**, 22504-22514.

72. B. R. Long, M. K. Y. Chan, J. P. Greeley and A. A. Gewirth, *J. Phys. Chem. C*, 2011, **115**, 18916-18921.

73. E. Durgun, N. Akman, C. Ataca and S. Ciraci, *Phys. Rev. B*, 2007, **76**, 245323.

74. A. Klamt and G. Schüürmann, *J. Chem. Soc., Perkin Trans. 2*, 1993, 799-805.

75. J. K. Nørskov, J. Rossmeisl, A. Logadottir, L. Lindqvist, J. R. Kitchin, T. Bligaard and H. Jónsson, *J. Phys. Chem. B*, 2004, **108**, 17886-17892.

76. J. Rossmeisl, A. Logadottir and J. K. Nørskov, *Chem. Phys.*, 2005, **319**, 178-184.

77. C. Kendrick, M.-W. Kuo, J. Li, H. Shen, T. S. Mayer and J. M. Redwing, *J. Appl. Phys.*, 2017, **122**, 235101.

78. S. P. Rodichkina, T. Nychyporuk, A. V. Pavlikov, V. Lysenko and V. Y. Timoshenko, *J. Raman Spectrosc.*, 2019, **50**, 1642-1648.

79. Y. Cui, X. Duan, J. Hu and C. M. Lieber, *J. Phys. Chem. B*, 2000, **104**, 5213-5216.

80. H. Peelaers, B. Partoens and F. M. Peeters, *Nano Lett.*, 2006, **6**, 2781-2784.

81. H.-J. Chun, V. Apaja, A. Clayborne, K. Honkala and J. Greeley, *ACS Catal.*, 2017, **7**, 3869-3882.

82. W. Nong, H. Liang, S. Qin, Y. Li and C. Wang, *ACS Appl. Mater. Interfaces*, 2020, **12**, 50505-50515.

83. Y. Yang, J. Liu, Z. Wei, S. Wang and J. Ma, *ChemCatChem*, 2019, **11**, 2821-2827.

84. X. Liu, Y. Jiao, Y. Zheng and S.-Z. Qiao, *ACS Catal.*, 2020, **10**, 1847-1854.

85. D. Jiao, Y. Liu, Q. Cai and J. Zhao, *J. Mater. Chem. A*, 2021, **9**, 1240-1251.

86. L. Li, J. M. P. Martirez and E. A. Carter, *ACS Catal.*, 2020, **10**, 12841-12857.

87. K. Peng, X. Wang and S.-T. Lee, *Appl. Phys. Lett.*, 2008, **92**, 163103.

88. C. K. Chan, H. Peng, G. Liu, K. McIlwrath, X. F. Zhang, R. A. Huggins and Y. Cui, *Nat. Nanotechnol.*, 2008, **3**, 31-35.

89. E. Peled, F. Patolsky, D. Golodnitsky, K. Freedman, G. Davidi and D. Schneier, *Nano Lett.*, 2015, **15**, 3907-3916.

90. X. Wang, G. Li, M. H. Seo, G. Lui, F. M. Hassan, K. Feng, X. Xiao and Z. Chen, *ACS Appl. Mater. Interfaces*, 2017, **9**, 9551-9558.